

Quantum phase transition without gap opening

X. M. Yang¹, G. Zhang² and Z. Song^{1*}

¹*School of Physics, Nankai University, Tianjin 300071, China*

²*College of Physics and Materials Science, Tianjin Normal University, Tianjin 300387, China*

Quantum phase transitions (QPTs), including symmetry breaking and topological types, always associated with gap closing and opening. We analyze the topological features of the quantum phase boundary of the XY model in a transverse magnetic field. Based on the results from graphs in the auxiliary space, we find that gapless ground states at boundary have different topological characters. On the other hand, In the framework of Majorana representation, the Majorana lattice is shown to be two coupled SSH chains. The analysis of the quantum fidelity for the Majorana eigen vector indicates the signature of QPT for the gapless state. Furthermore numerical computation shows that the transition between two types of gapless phases associates with divergence of second-order derivative of groundstate energy density, which obeys scaling behavior. It indicates that a continuous QPT can occur among gapless phases. The underlying mechanism of the gapless QPT is also discussed. The gap closing and opening are not necessary for a QPT.

I. INTRODUCTION

Understanding phase transitions is one of challenging tasks in condensed matter physics. No matter which types of a quantum phase transition (QPT), the groundstate wave function undergoes qualitative changes¹. There are various signature phenomena manifest the critical points, such as symmetry breaking, switch of topological invariant, divergence of entanglement, etc.. Among them, energy gap closing and opening seem never absent. It is important for a deeper understanding of QPTs to find out the role of the energy gap takes during the transition. Usually, a continuous QPT is characterized by a divergence in the second derivative of the groundstate energy density, assuming that the first derivative is discontinuous²⁻⁴. A natural question is whether the gap closing and opening are necessary for a QPT. The aim of this paper is to clarify the relation between gap and a second-order QPT through a concrete system. We take a 1D quantum XY model with a transverse field, which can be mapped onto the system of spinless fermions with p -wave superconductivity. It plays an important role both in traditional and symmetry-protected topological QPTs, received intense study in many aspects⁵⁻¹⁹.

The quantum phase boundary of the model is well known based on the exact solution. However, it mainly arises from the condition of zero energy gap. There are many other signatures to identify the critical point, such as the quantities of the ground state from the point of view of quantum information theory²⁰, the ground-state fidelity susceptibility^{7,21-27}. Then the ground states at different locations of the boundary may belong to different quantum phases, although they are not protected by a finite energy gap. In this paper, we are interested in the possible QPT along the boundary, at which the ground state is always gapless state. Our approach consists of three steps: Bogoliubov energy band, Majorana fidelity, and finite-size scaling. Firstly, we use Bogoliubov energy band to construct a group of graphs that can capture

the characters of quantum phases in every regions, including all the boundaries, which indicate the distinctions of boundaries. Secondly, we employ the fidelity of Majorana eigen vector to detect the QPT between two gapless phases. Thirdly, we investigate the scaling behavior of the critical region to show a gapless QPT has the same performance as a standard continuous QPT. The result indicates that a continuous QPT can occur among gapless phases. The gap closing and opening are not necessary for a QPT.

This paper is organized as follows. In Section II, we present the model Hamiltonian and the quantum phase diagram. In Section III, we investigate the phase diagram based on the geometric properties. Section IV gives the connection between the model to a simpler lattice model by Majorana transformation. In Section V, we present the scaling behavior about the groundstate energy density to demonstrate the characteristic of continuous QPT among the gapless phases. Finally, we give a summary and discussion in Section VI.

II. MODEL AND PHASE DIAGRAM

We consider a 1D spin-1/2 XY model in a transverse magnetic field λ on N -site lattice. The Hamiltonian has the form

$$H = \sum_{j=1}^N \left(\frac{1+\gamma}{2} \sigma_j^x \sigma_{j+1}^x + \frac{1-\gamma}{2} \sigma_j^y \sigma_{j+1}^y + \lambda \sigma_j^z \right), \quad (1)$$

where σ_j^α ($\alpha = \pm, z$) are the Pauli operators on site j , and satisfy the periodic boundary condition $\sigma_j^\alpha \equiv \sigma_{j+N}^\alpha$.

Now we consider the solution of the Hamiltonian of Eq. (1). We start by taking the Jordan-Wigner

transformation²⁸

$$\begin{aligned}\sigma_j^x &= -\prod_{i=1}^{j-1} (1 - 2c_i^\dagger c_i) (c_j^\dagger + c_j) \\ \sigma_j^y &= -i \prod_{i=1}^{j-1} (1 - 2c_i^\dagger c_i) (c_j^\dagger - c_j) \\ \sigma_j^z &= 1 - 2c_j^\dagger c_j\end{aligned}\quad (2)$$

to replace the Pauli operators by the fermionic operators c_j . The parity of the number of fermions

$$\Pi = \prod_{l=1}^N (\sigma_l^z) = (-1)^{N_p} \quad (3)$$

is a conservative quantity, i.e., $[H, \Pi] = 0$, where $N_p = \sum_{j=1}^N c_j^\dagger c_j$. Then the Hamiltonian (1) can be rewritten as

$$H = \sum_{\eta=+,-} P_\eta H_\eta P_\eta, \quad (4)$$

where

$$P_\eta = \frac{1}{2} (1 + \eta \Pi) \quad (5)$$

is the projector on the subspaces with even ($\eta = +$) and odd ($\eta = -$) N_p . The Hamiltonian in each invariant subspaces has the form

$$\begin{aligned}H_\eta &= \sum_{j=1}^{N-1} (c_j^\dagger c_{j+1} + \gamma c_j^\dagger c_{j+1}^\dagger) - \eta (c_N^\dagger c_1 + \gamma c_N^\dagger c_1^\dagger) \\ &+ \text{H.c.} - 2\lambda \sum_{j=1}^N c_j^\dagger c_j + N\lambda.\end{aligned}\quad (6)$$

Taking the Fourier transformation

$$c_j = \frac{1}{\sqrt{N}} \sum_{k_\pm} e^{ik_\pm j} c_{k_\pm}, \quad (7)$$

for the Hamiltonians H_\pm , we have

$$\begin{aligned}H_\eta &= -\sum_{k_\eta} [2(\lambda - \cos k_\eta) c_{k_\eta}^\dagger c_{k_\eta} \\ &+ i\gamma \sin k_\eta (c_{-k_\eta} c_{k_\eta} + c_{-k_\eta}^\dagger c_{k_\eta}^\dagger) - \lambda],\end{aligned}\quad (8)$$

where the momenta $k_+ = 2(m + 1/2)\pi/N$, $k_- = 2m\pi/N$, $m = 0, 1, 2, \dots, N-1$. Employing the Bogoliubov transformation

$$\gamma_{k_\eta} = \cos \theta_{k_\eta} c_{k_\eta}^\dagger + i \sin \theta_{k_\eta} c_{-k_\eta},$$

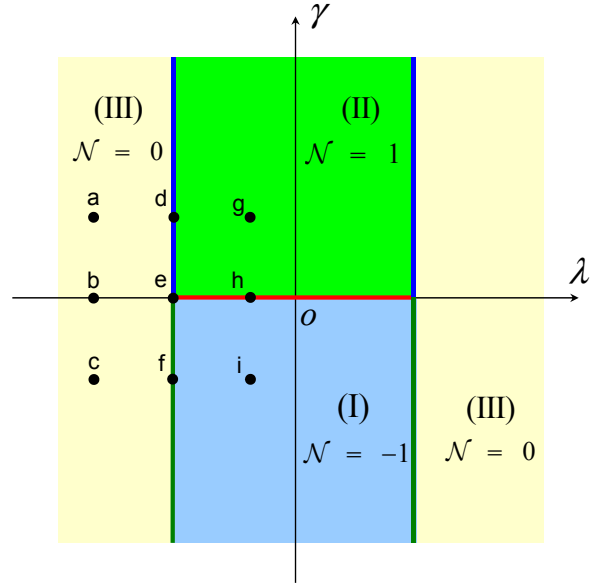


FIG. 1. (Color online) Phase diagram of the XY spin chain on the parameter $\lambda - \gamma$ plane. The blue lines indicate the boundary, which separate the phases with winding number 0 (yellow) and non-trivial topological phase with winding number 1 (green). The green lines separate the phases with winding number 0 (yellow) and non-trivial topological phase with winding number -1 (blue). The red line separate two phases with winding number 1 (green) and -1 (blue). Several points (a)–(i) at typical positions are indicated. The corresponding loops about the vector B are given in Fig. 2.

where

$$\tan(2\theta_{k_\eta}) = \frac{\gamma \sin k_\eta}{\lambda - \cos k_\eta}, \quad (9)$$

one can recast Hamiltonian H_η to the diagonal form

$$H_\eta = \sum_{k_\eta} \epsilon_{k_\eta} (\gamma_{k_\eta}^\dagger \gamma_{k_\eta} - \frac{1}{2}), \quad (10)$$

with spectrum being

$$\epsilon_{k_\eta} = 2\sqrt{(\lambda - \cos k_\eta)^2 + \gamma^2 \sin^2 k_\eta}. \quad (11)$$

The lowest energy in η subspace is $-\frac{1}{2} \sum_{k_\eta} \epsilon_{k_\eta}$ for $\lambda < 1$, while $-\frac{1}{2} \sum_{k_\eta} \epsilon_{k_\eta} + \frac{1-\eta}{2} \epsilon_0$ for $\lambda > 1$. The groundstate energy for finite N is the foundation for the analysis of scaling behavior in the Sec. V. In the thermodynamical limit, the difference between two subspaces can be neglected and the groundstate energy density can be expressed as

$$\varepsilon_g = -\frac{1}{4\pi} \int_{-\pi}^{\pi} \epsilon_k dk, \quad (12)$$

by taking $k = k_\eta$. The quantum phase boundary can be obtained from $\epsilon_k = 0$ as

$$\lambda = \pm 1, \text{ and } \gamma = 0 \text{ for } |\lambda| < 1. \quad (13)$$

The phase diagram is presented in Fig. 1. There are four regions separated by five lines as boundaries of quantum phases. In the next section, quantum phases and boundaries will be examined from the geometrical point of view.

III. TOPOLOGICAL INVARIANTS

In this section, we will investigate the topological characterization for the phase diagram. We demonstrate this point by rewriting the Hamiltonian in the form

$$H = \sum_{k>0} (c_k^\dagger \ c_{-k}) h_k \begin{pmatrix} c_k \\ c_{-k}^\dagger \end{pmatrix}, \quad (14)$$

where

$$h_k = 2 \begin{pmatrix} \cos k - \lambda & i\gamma \sin k \\ -i\gamma \sin k & \lambda - \cos k \end{pmatrix}. \quad (15)$$

The core matrix can be expressed as

$$h_k = \mathbf{B}(k) \cdot \sigma_k, \quad (16)$$

where the components of the auxiliary field $\mathbf{B}(k) = (B_x, B_y, B_z)$ are

$$\begin{cases} B_x = -2\gamma \sin k \\ B_y = 2 \cos k - 2\lambda \\ B_z = 0 \end{cases}. \quad (17)$$

The Pauli matrices $\sigma_{\mathbf{k}}$ are taken as the form

$$\sigma_x = \begin{pmatrix} 0 & -i \\ i & 0 \end{pmatrix}, \sigma_y = \begin{pmatrix} 1 & 0 \\ 0 & -1 \end{pmatrix}, \sigma_z = \begin{pmatrix} 0 & 1 \\ 1 & 0 \end{pmatrix}. \quad (18)$$

The winding number of a closed curve in the auxiliary $B_x B_y$ -plane around the origin is defined as

$$\mathcal{N} = \frac{1}{2\pi} \oint_C (\hat{B}_y d\hat{B}_x - \hat{B}_x d\hat{B}_y) \quad (19)$$

where the unit vector $\hat{\mathbf{B}}(k) = \mathbf{B}(k) / |\mathbf{B}(k)|$. \mathcal{N} is an integer representing the total number of times that curve travels counterclockwise around the origin. Actually, the winding number is simply related the loop described by equation

$$\frac{(B_x)^2}{4\gamma^2} + \frac{(B_y + 2\lambda)^2}{4} = 1, \quad (20)$$

which presents a normal ellipse in the $B_x B_y$ -plane. The shape and rotating direction of the ellipse dictated by the parameter equation (17) have the following symmetries. First of all, taking $\gamma \rightarrow -\gamma$, we have $[B_x(k), B_y(k)] \rightarrow [B_x(-k), B_y(-k)]$, representing

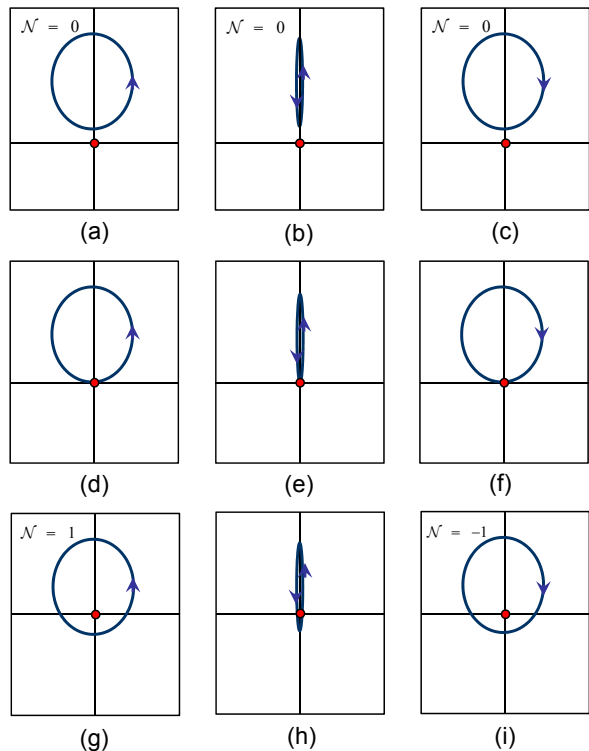


FIG. 2. (color online) Schematic illustration of nine types of phases by the geometry of graphs in the auxiliary $B_x B_y$ -plane. Red filled circle indicates the origin. (a), (b) and (c) present graphs of trivial topological phase with zero winding number. (g) and (i) present graphs of non-trivial topological phases with winding number ± 1 , which are separated by (h). (d), (e) and (f) are graphs of boundary. They correspond to ellipses with various shapes, but passing through the origin. We see that from (d) to (f), the graph becomes a segment. Although (d) and (f) have the same shape, they have opposite directions, indicating two different types of gapless phases.

the same ellipse but with opposite rotating direction. Secondly, taking $\lambda \rightarrow -\lambda$, we have $[B_x(k), B_y(k)] \rightarrow [B_x(k), B_y(k) + 4\lambda]$, representing the same ellipse but with a 4λ shift in B_y , while the 4λ shift cannot affect the relation between the graph and the origin. We plot several graphs at typical positions in Fig. 2 to demonstrate the features of different phases from the geometric point of view. We are interested in the loops for the parameters at the boundaries in Eq. (13). (i) For $\lambda = \pm 1$ and $\gamma \neq 0$, the ellipse always passes through the origin $(0,0)$ one time. Along the boundary, only the length of the semiaxis of the ellipse changes. (ii) For $\gamma = 0$ and $|\lambda| \leq 1$, the loop reduces to a segment, passing through the origin twice times. Along the boundary, only the length of the segment varies. According to the connection between loops and QPTs²⁹, when a loop passes through the origin, the first derivative of groundstate energy density experiences a non-analytical point. In general, this process is associated with a gap closing. However, we note that when parameters vary along $\lambda = \pm 1$ and pass

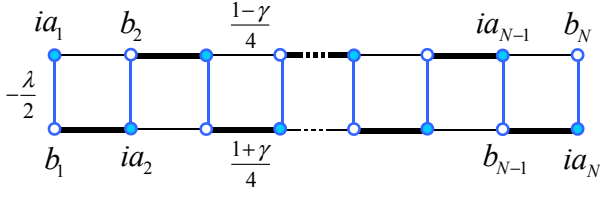


FIG. 3. (Color online) Lattice geometries for the Majorana Hamiltonian described in Eq. (26), Solid (empty) circle indicates (anti) Majorana modes. It represents two-coupled SSH chains.

through $\gamma = 0$, there is always one point in the curve at the origin, while the ellipse becomes a segment. In the Appendix, we show that such a system also experiences a non-analytical point but without associated gap closing and opening.

IV. MAJORANA LADDER

In this section, we investigate the phase diagram from alternative way, which gives a clear physical picture by connecting the obtained results to the previous work. In contrast to last section, where a graph is extracted from the Bogoliubov energy band, we will mark the phase diagram from the behavior of wave functions. For quantum spin model, Majorana representation always make things simpler since it can map a Kitaev model (like the form in Eq. (8)) to a lattice model in a real space with the twice number of site of the spin system³⁰. The bulk-edge correspondence has demonstrated this advantage³¹.

We introduce Majorana fermion operators

$$a_j = c_j^\dagger + c_j, b_j = -i(c_j^\dagger - c_j), \quad (21)$$

which satisfy the relations

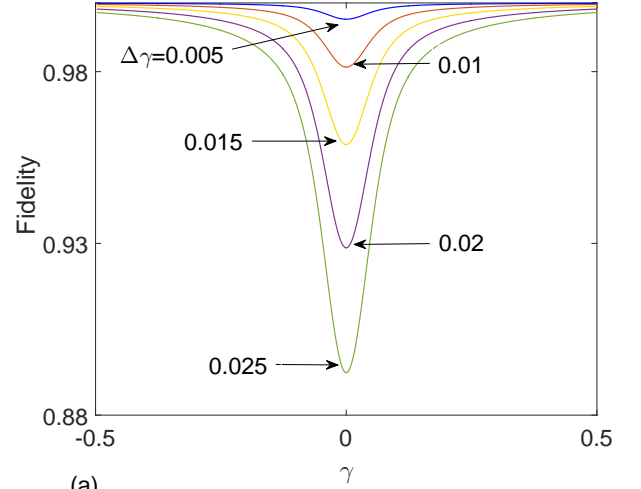
$$\begin{aligned} \{a_j, a_{j'}\} &= 2\delta_{j,j'}, \{b_j, b_{j'}\} = 2\delta_{j,j'}, \\ \{a_j, b_{j'}\} &= 0, a_j^2 = b_j^2 = 1. \end{aligned} \quad (22)$$

The inverse transformation is

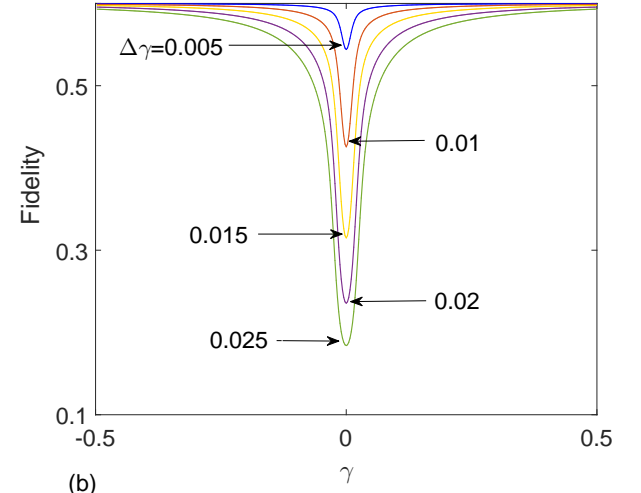
$$c_j^\dagger = \frac{1}{2}(a_j + ib_j), c_j = \frac{1}{2}(a_j - ib_j). \quad (23)$$

Then the Majorana representation of the Hamiltonian H_η is

$$\begin{aligned} H_\eta &= \frac{i}{4} \sum_{j=1}^{N-1} [(1+\gamma)b_j a_{j+1} + (1-\gamma)b_{j+1} a_j] \\ &\quad - \frac{i\eta}{4} [(1+\gamma)b_N a_1 + (1-\gamma)b_1 a_N] \\ &\quad + \frac{i\lambda}{2} \sum_{j=1}^N a_j b_j + \text{H.c.} \end{aligned} \quad (24)$$



(a)



(b)

FIG. 4. (Color online) The fidelity of the Majorana lattice with $\lambda = -1$ for the system with (a) $N = 20$, (b) $N = 100$ and various $\Delta\gamma$.

To make the structure of Majorana lattice clear, we write down the Hamiltonian in the basis $\varphi^T = (ia_1, b_1, ia_2, b_2, ia_3, b_3, \dots)$ and see that

$$H_\eta = \varphi^T h_\eta \varphi, \quad (25)$$

where h_η represents a $2N \times 2N$ matrix. Here matrix h_M is explicitly written as

$$\begin{aligned} h_\eta &= \frac{1}{4} \sum_{l=1}^{N-1} [(1+\gamma)|l, 2\rangle \langle l+1, 1| + (1-\gamma)|l+1, 2\rangle \langle l, 1|] \\ &\quad - \eta \frac{1}{4} [(1+\gamma)|N, 2\rangle \langle 1, 1| + (1-\gamma)|1, 2\rangle \langle N, 1|] \\ &\quad + \frac{\lambda}{2} \sum_{l=1}^N |l, 1\rangle \langle l, 2| + \text{H.c.} \end{aligned} \quad (26)$$

where basis $\{|l, \sigma\rangle, l \in [1, N], \sigma = 1, 2\}$ is an orthonormal complete set, $\langle l, \sigma | l', \sigma' \rangle = \delta_{ll'} \delta_{\sigma\sigma'}$. The

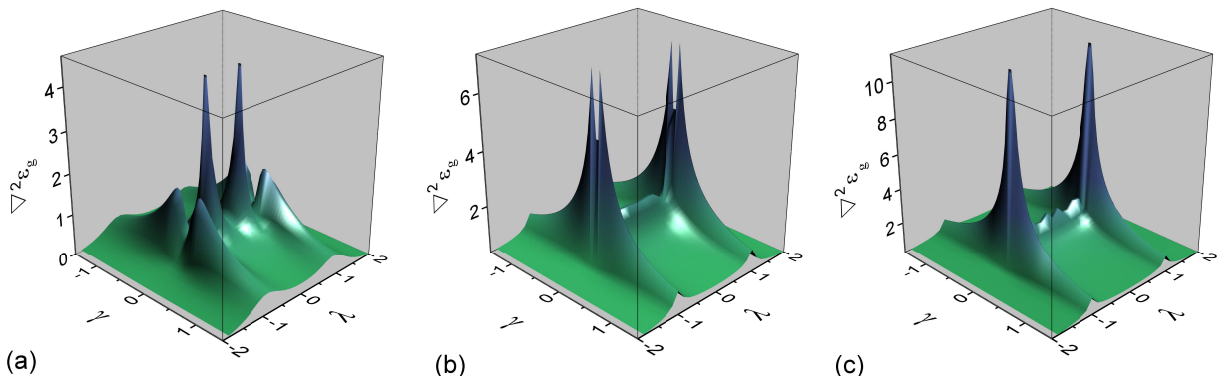


FIG. 5. (Color online) The Laplacian of the groundstate energy density ϵ_g as a function of the field for the case $N = 8, 40$ and 68 . The maxima (ridge) mark the pseudo-boundary quantum phases. We see that there are peaks on the ridge near the joints for the case of $N = 68$ (see also Fig. 6(a)).

basis array is $(|1, 1\rangle, |1, 2\rangle, |2, 1\rangle, |2, 2\rangle, \dots, |N-1, 1\rangle, |N-1, 2\rangle, |N, 1\rangle, |N, 2\rangle)$, which accords with φ^T . Schematic illustrations for structures of h_η are described in Fig. 3. The structure is clearly two coupled SSH chains. The situation with $\eta = +$ corresponds to the case with half quanta flux through the double SSH rings. In the previous work³², the gapless states in two coupled SSH chains with $\eta = -$ has been studied. It is shown that the quantum phase boundary $\gamma = 0$ for $|\lambda| < 1$ corresponds to topological gapless states, while boundaries $\lambda = \pm 1$ are trivial topological gapless states. The joints $(\gamma, \lambda) = (0, \pm 1)$ are boundaries separated the gapless phases with different topological characterizations. We refer these points as transition point between two gapless phases.

Majorana matrix in Eq. (26) with $2N$ dimension contains all the information of the original H in Eq. (1) with 2^N dimension. Although the eigen vectors of h_η have direct relation to the ground state of H , it is expected that the signature of QPT between gapless phases can be manifested from them. We will investigate the change of the eigen vector of h_+ along $\lambda = -1$. By the similar procedure, the eigen problem of the equation

$$h_+ |k_+, \rho\rangle = \epsilon_{k_+, \sigma} |k_+, \rho\rangle \quad (27)$$

with $\rho = \pm$, can be solved as

$$|k_+, \rho\rangle = \frac{1}{\sqrt{2N}} \sum_l (e^{ik_+l} |l, 1\rangle + \rho e^{-i\phi} e^{ik_+l} |l, 2\rangle), \quad (28)$$

with the eigen value

$$\epsilon_{k_+, \rho} = \frac{\rho}{2} \sqrt{(\cos k_+ + 1)^2 + (\gamma \sin k_+)^2}. \quad (29)$$

Here the parameter ϕ is defined as

$$\tan \phi = -\gamma \tan \frac{k_+}{2}. \quad (30)$$

We focus on the vectors $\{|k_+, -\rangle\}$ with negative eigen values and taking $|k_+, -\rangle = |k_+\rangle$.

We employ the quantum fidelity to detect the sudden change of the eigen vectors, which is defined as

$$F(\gamma, \Delta\gamma) = \prod_{k_+} O_{k_+} = \prod_{k_+} |\langle k_+(\gamma - \Delta\gamma) | k_+(\gamma + \Delta\gamma) \rangle|, \quad (31)$$

i.e., the modulus of the overlap between two neighbor vectors with $\gamma \pm \Delta\gamma$. Direct derivation shows that

$$\begin{aligned} O_{k_+} &\approx 1 - \frac{1}{2} \left| \frac{\partial |k_+(\gamma)\rangle}{\partial \gamma} \right|^2 (\Delta\gamma)^2 \\ &= 1 - \frac{\tan^2 \frac{k_+}{2}}{2 \left(1 + \gamma^2 \tan^2 \frac{k_+}{2}\right)^2} (\Delta\gamma)^2. \end{aligned} \quad (32)$$

We note that the minimum of O_{k_+} always locates at $\gamma = 0$ for any values of k_+ , leading to the minimum of $F(\gamma, \Delta\gamma)$. It indicates that the fidelity approach can be employed for Majorana eigen vector to witness the sudden change of ground state.

Fig. 4 shows the fidelity of h_+ for a given finite system as a function of γ with various parameter difference $\Delta\gamma$. As expected, the point $\gamma = 0$ is clearly marked by a sudden drop of the value of fidelity. The behavior can be ascribed to a dramatic change in the structure of the Majorana vector, indicating the QPT at zero γ .

V. SCALING BEHAVIOR

In this section, we investigate what happens for the groundstate energy when a gapless QPT occurs. The non-analytical point of energy density is more fundamental to judge the onset of a QPT. We start from the line with $\lambda = 1$, on which the density of groundstate energy in thermodynamic limit has the form

$$\epsilon_g^1 = -\frac{1}{\pi} \int_0^\pi \sqrt{(1 - \cos k)^2 + \gamma^2 \sin^2 k} dk, \quad (33)$$

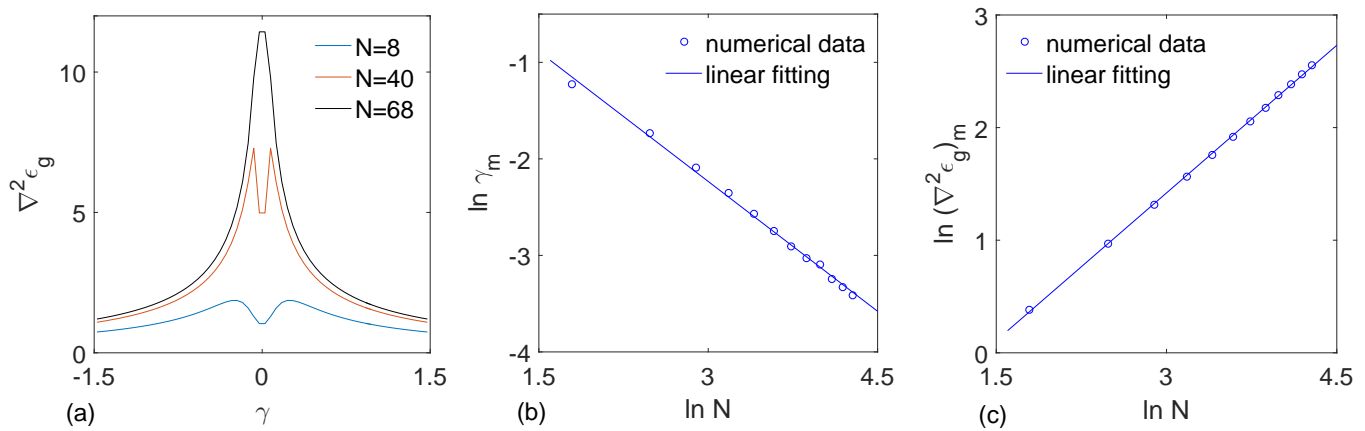


FIG. 6. (color online). The characteristics of second-order QPT for the present system. (a) Plots of $\nabla^2 \varepsilon_g$ as a function of γ for different values of N at $\lambda = 1$. (b) The scaling law of pseudo critical point γ_m as a function of N . (c) The scaling behavior for $(\nabla^2 \varepsilon_g)_m$, which is plotted as a function of N . The plots are fitted by solid lines $\ln \gamma_m = -0.897 \ln N + 0.456$ and $\ln (\nabla^2 \varepsilon_g)_m = 0.874 \ln N - 1.202$.

where we neglect the difference between k_+ and k_- . The first derivative of groundstate energy density with the respect to γ reads

$$\frac{\partial \varepsilon_g^1}{\partial \gamma} = \int_0^\pi F(k) dk \quad (34)$$

where the integrand is defined as

$$F(k) = -\frac{\gamma \sin^2 k}{\pi \sqrt{(1 - \cos k)^2 + \gamma^2 \sin^2 k}}. \quad (35)$$

We are interested in the divergent behavior of $\frac{\partial \varepsilon_g^1}{\partial \gamma}$ when $\gamma \sim 0$. We note that the main contribution to the integral of $\frac{\partial \varepsilon_g^1}{\partial \gamma}$ comes from the region $k \in [0, \delta]$ with $\delta \ll \pi$. The contribution to $\frac{\partial \varepsilon_g^1}{\partial \gamma}$ from this region is approximately

$$\int_0^\delta F(k) dk \approx \frac{4|\gamma|\gamma}{\pi} \left[1 - \sqrt{1 + \left(\frac{\delta}{2\gamma}\right)^2} \right], \quad (36)$$

which predicts that the first derivative of groundstate energy density along $\lambda = 1$ has a non-analytical point at $\gamma = 0$. It is the standard characterization of second order QPT. It is crucial to stress that such phase separation does not arise from the gap closing and opening.

To characterize the behavior of groundstate energy in 2D parameter space, we calculate the Laplacian of ε_g

$$\nabla^2 \varepsilon_g = \frac{\partial^2 \varepsilon_g}{\partial \lambda^2} + \frac{\partial^2 \varepsilon_g}{\partial \gamma^2}, \quad (37)$$

which will reduce to second derivative of the groundstate energy density of the standard transverse-field Ising model¹ with respect to the transverse field λ when we take $\gamma = 0$. In Fig. 5 we plot the Laplacian of ε_g

for the finite sized systems. We observe that as N increases, the regions of criticality are clearly marked by a sudden increase of the value of $\nabla^2 \varepsilon_g$. Remarkably, there are higher order sudden increases around the points $(\gamma, \lambda) = (0, \pm 1)$. As before in a conventional QPT with gap closing and opening, for instance the QPTs at $\lambda = \pm 1$ along $\gamma = 1$, we ascribe this type of behavior to a dramatic change in the structure of the gapless ground state. The system undergoes a QPT along the boundary.

In order to quantify the change of the ground state when the system crosses the critical point, we look at the value of $\nabla^2 \varepsilon_g$ as a function of (γ, λ) for finite size system. The results for systems of different size are presented in Fig. 6. We find the similar scaling behavior for such kinds of QPT, which reveals the fact that the signature of a second order QPT must not require the gap closing.

VI. SUMMARY AND DISCUSSION

In summary, we have studied the the necessity of the energy gap closing and opening for the presence of a QPT. We focused on the joint of three types of gapless phases. The analysis based on the geometry of the ground state and Majorana representation indicate the distinction of the gapless phases. Numerical computation for finite size system shows that the transitions among the gapless phases exhibit scaling behavior, which has been regarded as the fingerprint of continuous QPT. This provides an example to demonstrate that energy gap closing and opening is not a necessary condition for the QPT. Mathematically, the existence of a gap depends on the function of dispersion relation, specifically, the upper bound of the negative band. The divergence of the second-order derivative of groundstate energy density arises from the non-analytical point of the groundstate energy, which is the summation of all negative energy

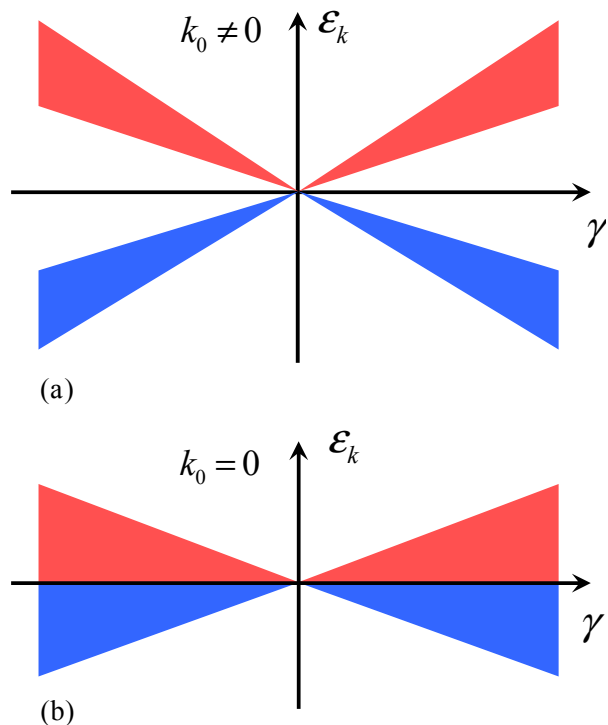


FIG. 7. (Color online) Energy spectra for the Hamiltonian $\sum h_k = \gamma(k + k_0)\sigma_x$ as a function of γ , with (a) $k_0 \neq 0$, and (b) $k_0 = 0$, respectively. We see that the groundstate energies of both cases have a non-analytical points at $\gamma = 0$. However, the gap closes only at $\gamma = 0$ in the case (a).

levels. On the other hand, a typical negative energy level with non-analytical point is a simple level crossing at zero energy, for example, levels from matrix $h_k = \gamma(k + k_0)\sigma_x$ for $k, k_0 \in [0, \pi]$. The energy gap $\Delta = 2\gamma k_0$, which is zero only at $\gamma = 0$, for nonzero k_0 . However, the energy gap always vanishes for zero k_0 . We plot the spectrum for $k_0 = 0$ and $k_0 \neq 0$, in Fig. 7 to illustrate this point.

VII. APPENDIX

In this appendix, we demonstrate the existence of gapless QPT through a toy model. We consider a Hamiltonian with a specific dispersion relation $\varepsilon_k = \sqrt{x^2(k) + y^2(k)}$ for Bogoliubov band, where $(x(k), y(k))$ describes a rectangle with width $2|\gamma|$ and length x_0 in

xy -plane (see Fig. 8). Here we use a rectangle to replace an ellipse in Eq. (20) in order to simplify the derivation. In the case of $x_0 \gg |\gamma|$, the main contribution to the energy is the ε_k at the long sides. The parameter equations of the two long sides is

$$\begin{cases} x = -|\gamma| \tan k, & (\theta_0 \leq k \leq \pi/2) \\ y = \pm\gamma, \end{cases} \quad (38)$$

where θ_0 is determined by $\tan\theta_0 = |\gamma|/x_0$. The energy

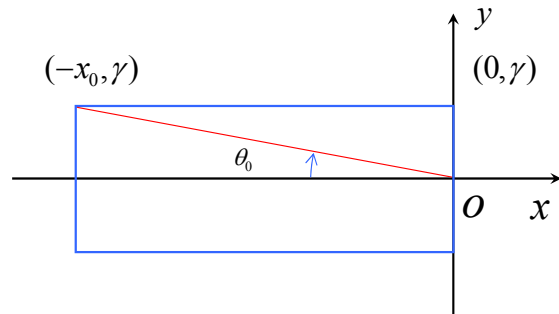


FIG. 8. (Color online) Schematics of a graph in auxiliary xy -plane for the Bogoliubov band of a toy model, which is a rectangle. As γ varies, the origin is always at one side of the rectangle, keeping the ground state fixed at gapless state.

density can be expressed as

$$\begin{aligned} \varepsilon &= -\frac{1}{\pi} \int_{\theta_0}^{\pi/2} \frac{|\gamma|}{\sin k} dk \\ &= \frac{|\gamma|}{\pi} \ln \tan(\theta_0/2) = \frac{|\gamma|}{\pi} \ln \frac{|\gamma|}{2x_0}. \end{aligned} \quad (39)$$

We note that the derivative of ε

$$\frac{\partial \varepsilon}{\partial \gamma} = \frac{\gamma}{\pi |\gamma|} \left(\ln \frac{|\gamma|}{2x_0} + 1 \right), \quad (40)$$

has a jump at zero γ , indicating the critical point of QPT.

ACKNOWLEDGMENTS

We acknowledge the support of the CNSF (Grant No. 11374163).

* songtc@nankai.edu.cn

¹ S. Sachdev, *Quantum Phase Transition* (Cambridge University Press, Cambridge, 1999).

² M. Vojta, Rep. Prog. Phys. **66**, 2069 (2003).

³ S. Suzuki, Inoue, J. I. and Chakrabarti, B. K. *Quantum Ising Phases and Transitions in Transverse Ising Models* Vol. 862 (Lecture Notes in Physics, Springer, 2013).

⁴ Dutta, *Quantum Phase Transitions in Transverse Field Spin Models: From Statistical Physics to Quantum Information* (Cambridge University Press, Cambridge, 2015)

⁵ G. Chen, J. Q. Li, and J. Q. Liang, Phys. Rev. A **74**, 054101 (2006).

⁶ X. X. Yi and W. Wang, Phys. Rev. A **75**, 032103 (2007).

- ⁷ L. C. Venuti and P. Zanardi, *Phys. Rev. Lett.* **99**, 095701 (2007).
- ⁸ Yu-Quan Ma and Shu Chen, *Phys. Rev. A* **79**, 022116 (2009).
- ⁹ Yu-Quan Ma, Shu Chen, Heng Fan, and Wu-Ming Liu, *Phys. Rev. B* **81**, 245129 (2010).
- ¹⁰ Tao Liu, Yu-Yu Zhang, Qing-Hu Chen, and Ke-Lin Wang, *Phys. Rev. A* **80**, 023810 (2009).
- ¹¹ Xiao-Zhong Yuan, Hsi-Sheng Goan, and Ka-Di Zhu, *Phys. Rev. A* **81**, 034102 (2010).
- ¹² Xiao-Ming Lu and Xiaoguang Wang, *Europhys. Lett.* **91**, 30003 (2010).
- ¹³ Sheng-Chang Li, Li-Bin Fu, and Jie Liu, *Phys. Rev. A* **84**, 053610 (2011).
- ¹⁴ Li-Da Zhang and Li-Bin Fu, *Europhys. Lett.* **93**, 30001 (2011).
- ¹⁵ Sheng-Chang Li and Li-Bin Fu, *Phys. Rev. A* **84**, 023605 (2011).
- ¹⁶ Zi-Gang Yuan, Ping Zhang, Shu-Shen Li, Jian Jing, and Ling-Bao Kong, *Phys. Rev. A* **85**, 044102 (2012).
- ¹⁷ A. C. M. Carollo and J. K. Pachos, *Phys. Rev. Lett.* **95**, 157203 (2005).
- ¹⁸ S. L. Zhu, *Phys. Rev. Lett.* **96**, 077206 (2006).
- ¹⁹ S. L. Zhu, *Int. J. Mod. Phys. B* **22**, 561 (2008).
- ²⁰ Osterloh, A., Amico, L., Falci, G. & Fazio, R., *Nature* **416**, 608–610, (2002).
- ²¹ Chandra, A. K., Das, A. and Chakrabarti, B. K., Vol. 802 (*Lecture Notes in Physics*, Springer, 2010).
- ²² C. De Grandi, V. Gritsev, and A. Polkovnikov, *Phys. Rev. B* **81**, 012303 (2010).
- ²³ S. Chen, L. Wang, Y. Hao, and Y. Wang, *Phys. Rev. A* **77**, 032111 (2008).
- ²⁴ A. Tribedi, and I. Bose, *Phys. Rev. A* **77**, 032307 (2008).
- ²⁵ Rams, M. M. and Damski, B., *Phys. Rev. Lett.* **106**, 055701 (2011).
- ²⁶ Cardy, J., *Phys. Rev. Lett.* **106**, 150404 (2011).
- ²⁷ Abanin, D. A. and Demler, E. *Phys. Rev. Lett.* **109**, 020504 (2012).
- ²⁸ P. Jordan and E. Wigner, *Z. Physik* **47**, 631 (1928).
- ²⁹ G. Zhang and Z. Song, *Phys. Rev. Lett.* **115**, 177204 (2015).
- ³⁰ A. Y. Kitaev, *Phys. Usp.* **44**, 131 (2001).
- ³¹ M. Z. Hasan and C. L. Kane, *Rev. Mod. Phys.* **82**, 3045 (2010).
- ³² C. Li, S. Lin, G. Zhang, and Z. Song, *Phys. Rev. B* **96**, 125418 (2017).